Preprints of the 21st IFAC World Congress (Virtual)
Berlin, Germany, July 12-17, 2020

Integrated Guidance and Control Using Adaptive Backstepping Approach for Maneuvering Target Interception ⋆

Pei Pei * **Yi Ji** * **Shaoming He** * **Jiang Wang** * **Defu Lin** *

* *School of Aerospace Engineering, Beijing Institute of Technology, Beijing 100081, China (e-mail: lindf@bit.edu.cn)*

Abstract: A novel approach to address the problem of integrated guidance and control(IGC) for a missile is studied in this paper. By taking target maneuver, aerodynamic uncertainty and fin servo dynamic uncertainty as external disturbances in the adaptive backstepping design procedure, the proposed controller requires no information on target maneuver and provides robustness against these uncertainties. Furthermore, the derivatives of the virtual control laws in the backstepping differentiation process are estimated by a smooth second-order sliding mode differentiator, this simplifies the calculation and avoids the explosion of terms phenomenon in the conventional backstepping method. The closed-loop stability of the overall system is supported by the Lyapunov stability theory. Numerical simulations of an air-to-air interception scenario are presented in the simulation part to verify the superior performance and the robustness of proposed IGC law.

Keywords: Backstepping method, Adaptive control, Integrated guidance and control

1. INTRODUCTION

The guidance and control of an interception missile are typically designed as a two-loop, one is the inner autopilot control loop and the other one is the outer guidance loop. The inner autopilot control loop is always simplified as a second-order system (Zarchan (2012)) and the outer guidance loop is designed separately. The lateral commands generated by outer guidance loop and tracked by the inner autopilot control loop. Different bandwidths and small inherent delay make it acceptable for intercepting target with low speed and weak maneuverability. However, with the increase of target maneuverability, the separate design approach significantly degrades the guidance performance (Wang et al. (2016a)).

To address the problem associated with classical guidance and control design, guidance law with autopilot dynamic compensation has been widely discussed (Zhou and Xu (2016); He et al. (2015b, 2017a)). These approaches may exhibit good performance by precisely compensating for the autopilot lag. However, performance will be degraded in the presence of system uncertainties.

In order to improve the performance of guidance and control, the IGC scheme has been widely studied in recent years. Methods, such as feedback linearization (Menon et al. (2004)), game-theoretic approach (Lin et al. (1992)), numerical state-dependent Riccati equation approach (Vaddi et al. (2009)), θ-D method (Xin et al. (2006)), sliding mode control (Phadke and Talole (2012)), L1 adaptive control (Erdos et al. (2012)), fuzzy logic control (Omar and Abido (2010)), time delay control (Park et al. (2011)), and continuous-time predictive control (Panchal et al. (2017)) have been discussed in IGC design.

Besides previous approaches, the backstepping technique has been widely used for the IGC controller design. The strict-feedback form of interception engagement can be established for the backstepping design process under some reasonable assumptions (Zhang and Song (2009)). Backstepping method and input-to-state stability theory (Fei et al. (2015)) were used in IGC law design in the presence of actuator failures, and the robustness of the control law was proved. However, in the application process, the existence of "explosion of terms" cannot be avoided because of the analytic differentiation of virtual control laws. To overcome the inherent drawback of backstepping design, the dynamic surface theory was implemented in the IGC controller design (Hou et al. (2013); Wang et al. (2016b)). This approach substituted the analytic differentiation by the low-pass filter. However, this approach only considered a target with weak maneuverability. An adaptive fuzzy dynamic surface control based IGC controller (Ran et al. (2014)) was proposed to enhance the performance of dynamic surface control based IGC controller. In this approach, the uncertainties and target maneuver were compensated by an online adaptive fuzzy system. However, it was too complicated and time-consuming.

In this paper, a novel IGC controller is proposed for maneuvering target interception without knowing the target information. Target maneuvering, aerodynamic uncertainty, and fin servo uncertainty are treated as external disturbances and compensated by adaptive laws. Different from the dynamic surface control based controller, the derivatives of virtual control laws are esti-

⋆ This work was supported by the National Natural Science Foundation of China under Grant U1613225.

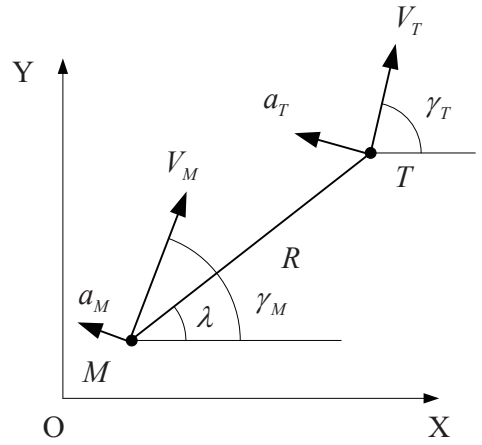

Fig. 1. Terminal phase geometry of interception

mated by a smooth second-order sliding mode differentiator (SSOSMD). The overall closed-loop stability analysis demonstrates that the tracking error can be bounded arbitrarily small by proper parameter designing. Finally, the effectiveness and robustness of the proposed IGC law are verified by comparison simulation results.

The rest of this paper is organized as follows. Sec 2 formulates the problem. The IGC controller and SSOSMD are derived in Sec 3. Then the closed-loop stability analysis is shown in Sec 4, followed by some comparison numerical simulations in Sec 5.1. Finally, Sec 6 concludes this work.

2. PROBLEM FORMULATION

Considering the terminal phase of intercepting a maneuvering target. Fig.1 shows the geometry of the terminal phase interception. The missile and target are assumed as point masses. We denote the missile and target by the subscripts M and T, respectively. The speed, normal acceleration, flight-path angle, missile and target range, and line-of-sight (LOS) angle are denoted by V, a, γ, R, and λ, respectively.

The kinematics of engagement can be expressed as (He et al. (2015a))

$$\ddot{R} = R\dot{\lambda}^2 + a_{Tr} - a_{Mr} \tag{1}$$

$$\ddot{\lambda} = -\frac{2\dot{R}\dot{\lambda}}{R} + \frac{a_{T\lambda}}{R} - \frac{a_{M\lambda}}{R} \tag{2}$$

where $a_{Mr} = a_M \sin(\lambda - \gamma_M)$ and $a_{Tr} = a_T \sin(\lambda - \gamma_T)$ denote the acceleration of missile and target along the LOS, $a_{M\lambda} = a_M \cos(\lambda - \gamma_M)$ and $a_{T\lambda} = a_T \cos(\lambda - \gamma_T)$ are the acceleration of missile and target perpendicular to the LOS, respectively.

The missile considered here is a roll stabilized, and a skid-to-turn missile with the cruciform tail-control surface. The dynamic equations of the missile can be expressed as (Yan et al. (2014); Ran et al. (2014); Wei et al. (2010))

$$\begin{cases} \dot{\alpha} = \dfrac{1}{mV_M}(-L + mg\cos\gamma_M) + \omega_z \\ \dot{\omega}_z = \dfrac{M}{J_z} \\ \dot{\theta} = \omega_z \\ \alpha = \theta - \gamma_M \end{cases} \tag{3}$$

where α is the angle of attack, g is the gravitational acceleration, m, ω_z, J_z and θ are the mass, pitch angular rate, inertia moment, and pitch angle of the missile, respectively. L is the aerodynamic lift fore and M is the aerodynamic pitch moment, which can be formulated as (Yan et al. (2014); Ran et al. (2014); Wei et al. (2010))

$$\begin{cases} L = Qsc_y^{\alpha}\alpha + Qsc_y^{\delta_z}\delta_z \\ M = Qslm_z^{\alpha}\alpha + Qslm_z^{\delta_z}\delta_z + \dfrac{Qsl^2m_z^{\omega_z}}{V_M}\omega_z \end{cases} \tag{4}$$

where Q is the dynamic pressure, s, l, and δ_z are the reference area, reference length, and the fin deflection angle of the missile, respectively. c_y^{α} and $c_y^{\delta_z}$ are the aerodynamic lift force derivative with respect to α and δ_z, respectively. m_z^{α}, $m_z^{\delta_z}$, and $m_z^{\omega_z}$ are the pitch moment derivative with respect to α, δ_z, and ω_z, respectively.

Substituting (4) into (3) yields

$$\begin{cases} \dot{\alpha} = -C_y^{\alpha}\alpha - C_y^{\delta_z}\delta_z + \omega_z + \dfrac{g\cos\gamma_M}{V_M} \\ \dot{\omega}_z = M_z^{\alpha}\alpha + M_z^{\delta_z}\delta_z + M_z^{\omega_z}\omega_z \\ \dot{\theta} = \omega_z \\ \alpha = \theta - \gamma_M \end{cases} \tag{5}$$

where the aerodynamic coefficients are

$$C_y^{\alpha} = \frac{Qsc_y^{\alpha}}{mV_M}, C_y^{\delta_z} = \frac{Qsc_y^{\delta_z}}{mV_M}, M_z^{\alpha} = \frac{Qslm_z^{\alpha}}{J_z}, M_z^{\delta_z} = \frac{Qslm_z^{\delta_z}}{J_z},$$
$$M_z^{\omega_z} = \frac{Qsl^2m_z^{\omega_z}}{J_zV_M}$$

The normal acceleration of missile can be derived from (5) as (He et al. (2017b))

$$\begin{aligned} a_M &= V_M\dot{\gamma}_M = V_M\left(\dot{\theta} - \dot{\alpha}\right) \\ &= V_M\left(C_y^{\alpha}\alpha + C_y^{\delta_z}\delta_z\right) - g\cos\gamma_M \end{aligned} \tag{6}$$

While the aerodynamic coefficients are derived from wind-tunnel experiments. The real value may dispersion from the nominal value, the aerodynamic uncertainties should be take into consideration. Therefore, the aerodynamic coefficients can be formulated as

$$\begin{aligned} &C_y^{\alpha} = C_{y,n}^{\alpha} + C_{y,u}^{\alpha}, C_y^{\delta_z} = C_{y,n}^{\delta_z} + C_{y,u}^{\delta_z} \\ &M_z^{\alpha} = M_{z,n}^{\alpha} + M_{z,u}^{\alpha}, M_z^{\delta_z} = M_{z,n}^{\delta_z} + M_{z,u}^{\delta_z} \\ &M_z^{\omega_z} = M_{z,n}^{\omega_z} + M_{z,u}^{\omega_z} \end{aligned} \tag{7}$$

where the parameters with subscripts n, u denote the nominal and bounded uncertain values of the corresponding aerodynamic coefficients, respectively.

In practice, the fin servo dynamic is formulated as (Idan et al. (2007))

$$\dot{\delta}_z = -\frac{1}{\tau_s}\delta_z + \frac{1}{\tau_s}\delta_{zc} \tag{8}$$

where δ_{zc} denotes the fin deflection angle command.

3. INTEGRATED GUIDANCE AND CONTROL DESIGN

The control law we designed here is to derive the fin deflection angle command to nullify the LOS angular rate $\dot{\lambda}$, because nullifies the LOS angular rate $\dot{\lambda}$ will lead to zero miss distance. Following the backstepping design method, the design processes are designed as follows.

Step 1: Define the sliding surface as $s_1 = \left(R/V_M C_{y,n}^{\alpha}\right)(\dot{\lambda} - 0)$, differentiating s_1 with respect to time yields

$$\begin{aligned}\dot{s}_1 &= \frac{-\dot{R}\dot{\lambda} + a_{T\lambda} - a_M \cos(\lambda - \gamma_M)}{V_M C_{y,n}^{\alpha}} \\ &= \frac{-\dot{R}\dot{\lambda} + a_{T\lambda} - V_M\left(C_y^{\alpha}\alpha + C_y^{\delta_z}\delta_z\right)\cos(\lambda - \gamma_M)}{V_M C_{y,n}^{\alpha}} \\ &\quad + \frac{g\cos\gamma_M \cos(\lambda - \gamma_M)}{V_M C_y^{\alpha}}\end{aligned} \tag{9}$$

Note that the target maneuver profile is unknown. Let $\Delta_1 = \left(a_{T\lambda} - V_M\left(C_y^{\delta_z}\delta_z + C_{y,u}^{\alpha}\right)\cos(\lambda - \gamma_M)\right)/V_M C_{y,n}^{\alpha}$ be an external disturbance. Δ_1 satisfies $|\Delta_1| \le M_1$, where M_1 is an unknown positive constant. Then, the (9) becomes:

$$\begin{aligned}\dot{s}_1 = &-\frac{\dot{R}\dot{\lambda}}{V_M C_{y,n}^{\alpha}} - \alpha\cos(\lambda - \gamma_M) \\ &+ \frac{g\cos\gamma_M\cos(\lambda - \gamma_M)}{V_M C_{y,n}^{\alpha}} + \Delta_1\end{aligned} \tag{10}$$

For subsystem (10), design the following virtual control law

$$\alpha^* = \frac{1}{\cos(\lambda - \gamma_M)}\left(\begin{array}{l}\dfrac{g\cos\gamma_M\cos(\lambda - \gamma_M)}{V_M C_{y,n}^{\alpha}} + k_1 s_1 \\ +\hat{M}_1\mathrm{sgn}(s_1) - \dfrac{\dot{R}\dot{\lambda}}{V_M C_{y,n}^{\alpha}}\end{array}\right) \tag{11}$$

where $k_1 > 0$. The adaptive control law is designed as:

$$\dot{\hat{M}}_1 = r_1|s_1| - \rho_1\hat{M}_1 \tag{12}$$

where $r_1 > 0$ and $\rho_1 > 0$.

Step 2: Define the sliding surface as $s_2 = \alpha - \alpha^*$, differentiating s_2 with respect to time yields

$$\begin{aligned}\dot{s}_2 &= \dot{\alpha} - \dot{\alpha}^* \\ &= -C_y^{\alpha}\alpha - C_y^{\delta_z}\delta_z + \frac{g\cos\gamma_M}{V_M} + \omega_z - \dot{\alpha}^*\end{aligned} \tag{13}$$

Let $\Delta_2 = -C_{y,u}^{\alpha}\alpha - C_y^{\delta_z}\delta_z$ be an external disturbance. Δ_2 satisfies $|\Delta_2| \le M_2$, where M_2 is an unknown positive constant. Then, (13) becomes

$$\dot{s}_2 = -C_{y,n}^{\alpha}\alpha + \frac{g\cos\gamma_M}{V_M} + \omega_z - \dot{\alpha}^* + \Delta_2 \tag{14}$$

For subsystem (14), design the following virtual control law

$$\begin{aligned}\omega_z^* = &C_{y,n}^{\alpha}\alpha - \frac{g\cos\gamma_M}{V_M} + \cos(\lambda - \gamma_M)s_1 + \dot{\alpha}^* \\ &- k_2 s_2 - \hat{M}_2\mathrm{sgn}(s_2)\end{aligned} \tag{15}$$

where $k_2 > 0$. The adaptive control law is designed as:

$$\dot{\hat{M}}_2 = r_2|s_2| - \rho_2\hat{M}_2 \tag{16}$$

where $r_2 > 0$ and $\rho_2 > 0$.

Step 3: Define the sliding surface as $s_3 = \omega_z - \omega_z^*$, differentiating s_3 with respect to time yields

$$\begin{aligned}\dot{s}_3 &= \dot{\omega}_z - \dot{\omega}_z^* \\ &= M_z^{\alpha}\alpha + M_z^{\delta_z}\delta_z + M_z^{\omega_z}\omega_z - \dot{\omega}_z^*\end{aligned} \tag{17}$$

Let $\Delta_3 = M_{z,u}^{\alpha}\alpha + M_{z,u}^{\delta_z}\delta_z + M_{z,u}^{\omega_z}\omega_z$ be an external disturbance. Δ_3 satisfies $|\Delta_3| \le M_3$, where M_3 is an unknown positive constant. Then, (17) becomes

$$\dot{s}_3 = M_{z,n}^{\alpha}\alpha + M_{z,n}^{\delta_z}\delta_z + M_{z,n}^{\omega_z}\omega_z - \dot{\omega}_z^* + \Delta_3 \tag{18}$$

For subsystem (18), design a following virtual control law

$$\delta_z^* = \frac{1}{M_{z,n}^{\delta_z}}\left(\begin{array}{l}-M_{z,n}^{\alpha}\alpha - M_{z,n}^{\omega_z}\omega_z - s_2 + \dot{\omega}_z^* \\ -k_3 s_3 - \hat{M}_3\mathrm{sgn}(s_3)\end{array}\right) \tag{19}$$

where $k_3 > 0$. The adaptive control law is designed as:

$$\dot{\hat{M}}_3 = r_3|s_3| - \rho_3\hat{M}_3 \tag{20}$$

where $r_3 > 0$ and $\rho_3 > 0$.

Step 4: Define the sliding surface as $s_4 = \delta_z - \delta_z^*$, differentiating s_4 with respect to time yields

$$\begin{aligned}\dot{s}_4 &= \dot{\delta}_z - \dot{\delta}_z^* \\ &= -\frac{1}{\tau_s}\delta_z + \frac{1}{\tau_s}\delta_{zc} - \dot{\delta}_z^*\end{aligned} \tag{21}$$

Suppose that $\delta_z = \delta_{z,n} + \delta_{z,u}$, $\delta_{z,n}$ denotes the nominal value of fin deflection, $\delta_{z,u}$ denotes the bounded fin servo dynamics uncertainty. Let $\Delta_4 = \delta_{z,u}/\tau_s$ be an external disturbance. Therefore, Δ_4 satisfies $|\Delta_4| \le M_4$, where M_4 is an unknown positive constant. Then, (21) becomes

$$\dot{s}_4 = -\frac{1}{\tau_s}\delta_{z,n} + \frac{1}{\tau_s}\delta_{zc} - \dot{\delta}_z^* + \Delta_4 \tag{22}$$

Finally, for the subsystem (22), design the following control law

$$\delta_{zc} = \delta_{z,n} + \tau_s\dot{\delta}_z^* - \tau_s M_z^{\delta_z}s_3 - \tau_s k_4 s_4 - \tau_s\hat{M}_4\mathrm{sgn}(s_4) \tag{23}$$

where $k_4 > 0$. The adaptive control law is designed as:

$$\dot{\hat{M}}_4 = r_4|s_4| - \rho_4\hat{M}_4 \tag{24}$$

where $r_4 > 0$ and $\rho_4 > 0$.

The first term on the right hand of (12), (16), (20) and (24) are used to estimate the external disturbance, and the second term attenuates the overestimation of external disturbance. Different from (Panchal et al. (2017); Shima et al. (2006); Shtessel and Tournes (2009); Erdos et al. (2012)), the proposed control law (23) requires no target maneuvering information to design the series of adaptive gains. The adaptive terms contribute to the robustness of the control law to against the target maneuver. Therefore, the proposed IGC control law is more practical. In addition, the derivative of α^*, ω_z^*, and δ_z^* cannot be analytical calculated due to the complicated forms of (11), (15), and (19). An SSOSMD is proposed here to estimate the precise values of $\dot{\alpha}^*$, $\dot{\omega}_z^*$, and $\dot{\delta}_z^*$. Taking $\dot{\alpha}^*$ as an example, formulate the differentiator as follows

$$\left\{\begin{array}{l}\dot{\hat{\alpha}}^* = \hat{\alpha}^* + \tau_1|\alpha^* - \hat{\alpha}^*|^{1-1/p}\mathrm{sgn}(\alpha^* - \hat{\alpha}^*) \\ \qquad +\tau_2|\alpha^* - \hat{\alpha}^*|^{1+1/p}\mathrm{sgn}(\alpha^* - \hat{\alpha}^*) \\ \dot{\hat{\alpha}}^* = \tau_3|\alpha^* - \hat{\alpha}^*|^{1-2/p}\mathrm{sgn}(\alpha^* - \hat{\alpha}^*) \\ \qquad +\tau_4\tau_3|\alpha^* - \hat{\alpha}^*|^{1+2/p}\mathrm{sgn}(\alpha^* - \hat{\alpha}^*)\end{array}\right. \tag{25}$$

where $\hat{\alpha}^*$ and $\dot{\hat{\alpha}}^*$ are the estimations of α^* and $\dot{\alpha}^*$, respectively. The design parameter $\tau_1, \tau_2, \tau_3, \tau_4 > 0$ and $p > 2$.

Theorem 1. Let $e_1 = \alpha^* - \hat{\alpha}^*$ and $e_2 = \dot{\alpha}^* - \dot{\hat{\alpha}}^*$ be the estimation errors. Then, the estimation errors can converge to a small region around zero if α^* satisfies $|\ddot{\alpha}^*| \leq L$, L is a constant value.

Proof. The SSOSMD error system is obtained as

$$\begin{cases} \dot{e}_1 = \dot{\alpha}^* - \dot{\hat{\alpha}}^* \\ \quad = e_2 - \tau_1 |e_1|^{1-1/p} \mathrm{sgn}\,|e_1| - \tau_2 |e_1|^{1+1/p} \mathrm{sgn}\,|e_1| \\ \dot{e}_2 = \ddot{\alpha}^* - \dot{\hat{\alpha}}^* \\ \quad = \ddot{\alpha}^* - \tau_3 |e_1|^{1-2/p} \mathrm{sgn}\,|e_1| - \tau_4 |e_1|^{1+2/p} \mathrm{sgn}\,|e_1| \end{cases} \tag{26}$$

For system (26), consider the following Lyapunov function candidate

$$W = \frac{1}{2} e_1^2 + \frac{1}{2} e_2^2 \tag{27}$$

Differentiating W with respect to time, and according to the Young's inequality, the equation can be simplified as

$$\begin{aligned} \dot{W} &= e_1 \left(e_2 - \tau_1 |e_1|^{1-1/p} \mathrm{sgn}\,|e_1| - \tau_2 |e_1|^{1+1/p} \mathrm{sgn}\,|e_1| \right) \\ &\quad + e_2 \left(\ddot{\alpha}^* - \tau_3 |e_1|^{1-2/p} \mathrm{sgn}\,|e_1| - \tau_4 |e_1|^{1+2/p} \mathrm{sgn}\,|e_1| \right) \\ &\leq \frac{1}{2} e_1^2 + e_2^2 + \frac{1}{2} \ddot{\alpha}^{*2} - 2\sqrt{\tau_1 \tau_2} e_1^2 - \frac{\sqrt{\tau_3 \tau_4}}{2} \left(e_1^2 + e_2^2 \right) \\ &= - \left(-\frac{1}{2} + 2\sqrt{\tau_1 \tau_2} + \frac{\sqrt{\tau_3 \tau_4}}{2} \right) e_1^2 - \left(\frac{\sqrt{\tau_3 \tau_4}}{2} - 1 \right) e_2^2 + \frac{1}{2} L^2 \\ &\leq -aW + \frac{1}{2} L^2 \end{aligned} \tag{28}$$

where

$$a = \min \left\{ -\frac{1}{2} + 2\sqrt{\tau_1 \tau_2} + \frac{\sqrt{\tau_3 \tau_4}}{2}, \frac{\sqrt{\tau_3 \tau_4}}{2} - 1 \right\}$$

the differential inequality can be solved during the time domain $[0, t]$

$$0 \leq W(t) \leq \left[W(0) - \frac{L^2}{2a} \right] e^{-at} + \frac{L^2}{2a} \tag{29}$$

where $W(0)$ denotes the initial value of W. By properly setting the parameters we can make ensure that $a > 0$. Note that if $W(0) \leq L^2/2a$, the upper bound of $W(t)$ is $L^2/2a$. Therefore the upper bound can be arbitrarily small by designing proper parameters. The error states e_1 and e_2 will converge to a small region around zero due to the positive definitive of all terms in (27). If $W(0) > L^2/2a$, then $\dot{W}(0) < 0$, which means that the W is monotone decreasing. If W satisfies $W > L^2/2a$ and $\forall t \in [0, t_f]$, then $\dot{W} < 0$ holds. This means that the system is Lyapunov stable. When W decrease to $W \leq L^2/2a$, the problem reduces to the first case that has been discussed above. Finally, we can conclude that the estimation errors can converge to a small enough region around zero. This completes the proof.

Since the upper bound can be arbitrarily small, the estimation errors can be restricted to a small region around zero, generating precisely estimation.

4. STABILITY ANALYSIS

According to the control law derived processes, the closed-loop system can be defined as

$$\begin{aligned} \dot{s}_1 &= -\cos(\lambda - \gamma_M) s_2 - k_1 s_1 - \hat{M}_1 \mathrm{sgn}(s_1) + \Delta_1 \\ \dot{s}_2 &= s_3 + \cos(\lambda - \gamma_M) s_1 - k_2 s_2 - \hat{M}_2 \mathrm{sgn}(s_2) + \dot{\hat{\alpha}}^* - \dot{\alpha}^* \\ &\quad + \Delta_2 \\ \dot{s}_3 &= M_{z,n}^{\delta_z} s_4 - s_2 - k_3 s_3 - \hat{M}_3 \mathrm{sgn}(s_3) + \dot{\hat{\omega}}_z^* - \dot{\omega}_z^* + \Delta_3 \\ \dot{s}_4 &= -M_{z,n}^{\delta_z} s_3 - k_4 s_4 - \hat{M}_4 \mathrm{sgn}(s_4) + \dot{\hat{\delta}}_z^* - \dot{\delta}_z^* + \Delta_4 \end{aligned} \tag{30}$$

Consider the following Lyapunov function candidate:

$$\begin{aligned} V =& \frac{1}{2} s_1^2 + \frac{1}{2} s_2^2 + \frac{1}{2} s_3^2 + \frac{1}{2} s_4^2 + \frac{1}{2r_1} \tilde{M}_1^2 \\ &+ \frac{1}{2r_2} \tilde{M}_2^2 + \frac{1}{2r_3} \tilde{M}_3^2 + \frac{1}{2r_4} \tilde{M}_4^2 \end{aligned} \tag{31}$$

where $\tilde{M}_i = M_i - \hat{M}_i$, $i = 1, 2, 3, 4$ are the estimation errors of external disturbances. Differentiating V yields

$$\begin{aligned} \dot{V} =& s_1 \left(-k_1 s_1 - \hat{M}_1 \mathrm{sgn}(s_1) + \Delta_1 \right) \\ &+ s_2 \left(-k_2 s_2 - \hat{M}_2 \mathrm{sgn}(s_2) + \dot{\hat{\alpha}}^* - \dot{\alpha}^* + \Delta_2 \right) \\ &+ s_3 \left(-k_3 s_3 - \hat{M}_3 \mathrm{sgn}(s_3) + \dot{\hat{\omega}}_z^* - \dot{\omega}_z^* + \Delta_3 \right) \\ &+ s_4 \left(-k_4 s_4 - M_4 \mathrm{sgn}(s_4) + \dot{\hat{\delta}}_z^* - \dot{\delta}_z^* + \Delta_4 \right) \\ &+ \frac{\tilde{M}_1}{r_1} \left(-r_1 |s_1| + \rho_1 \hat{M}_1 \right) + \frac{\tilde{M}_2}{r_2} \left(-r_2 |s_2| + \rho_2 \hat{M}_2 \right) \\ &+ \frac{\tilde{M}_3}{r_3} \left(-r_3 |s_3| + \rho_3 \hat{M}_3 \right) + \frac{\tilde{M}_4}{r_4} \left(-r_4 |s_4| + \rho_4 \hat{M}_4 \right) \\ \leq& -k_1 s_1^2 - k_2 s_2^2 - k_3 s_3^2 - k_4 s_4^2 \\ &+ s_2 \left(\dot{\hat{\alpha}}^* - \dot{\alpha}^* \right) + s_3 \left(\dot{\hat{\omega}}_z^* - \dot{\omega}_z^* \right) + s_4 \left(\dot{\hat{\delta}}_z^* - \dot{\delta}_z^* \right) \\ &+ \frac{\rho_1}{r_1} \tilde{M}_1 \hat{M}_1 + \frac{\rho_2}{r_2} \tilde{M}_2 \hat{M}_2 + \frac{\rho_3}{r_3} \tilde{M}_3 \hat{M}_3 + \frac{\rho_4}{r_4} \tilde{M}_3 \hat{M}_3 \end{aligned} \tag{32}$$

Note that $\tilde{M}_i \hat{M}_i = \tilde{M}_i \left(M_i - \tilde{M}_i \right) \leq \left(M_i^2 - \tilde{M}_i^2 \right)/2$, the (32) can be simplified as

$$\begin{aligned} \dot{V} \leq& -k_1 s_1^2 - k_2 s_2^2 - k_3 s_3^2 - k_4 s_4^2 + \frac{s_2^2 + \left(\dot{\hat{\alpha}}^* - \dot{\alpha}^* \right)^2}{2} \\ &+ \frac{s_3^2 + \left(\dot{\hat{\omega}}_z^* - \dot{\omega}_z^* \right)^2}{2} + \frac{s_4^2 + \left(\dot{\hat{\delta}}_z^* - \dot{\delta}_z^* \right)^2}{2} \\ &+ \frac{\rho_1}{2r_1} \left(M_1^2 - \tilde{M}_1^2 \right) + \frac{\rho_2}{2r_2} \left(M_2^2 - \tilde{M}_2^2 \right) \\ &+ \frac{\rho_3}{2r_3} \left(M_3^2 - \tilde{M}_3^2 \right) + \frac{\rho_4}{2r_4} \left(M_4^2 - \tilde{M}_4^2 \right) \\ \leq& -c_1 V + c_2 \end{aligned} \tag{33}$$

where

$$c_1 = \min \left\{ k_1, k_2 - \frac{1}{2}, k_3 - \frac{1}{2}, k_4 - \frac{1}{2}, \rho_1, \rho_2, \rho_3, \rho_4 \right\}$$

By choosing proper parameters, we can ensure that $c_1 > 0$ and $c_2 > 0$. Solving inequality (33) yields

$$0 \leq V(t) \leq \left[V(0) - \frac{c_2}{c_1} \right] e^{-c_1 t} + \frac{c_2}{c_1} \tag{34}$$

where $V(0)$ is the initial value of V. Note that if $V(0) \leq c_2/c_1$, the upper bound of $V(t)$ is c_2/c_1, and the upper bound can be arbitrarily small by designing proper parameters. The system state s_1 will converge to a small

region around zero due to the positive definitive of all terms in (31). This indicates that the LOS angular rate will converge to zero. If $V(0) > c_2/c_1$, then $\dot{V}(0) < 0$, which means that V is monotone decreasing. If V satisfies $V > c_2/c_1$ for all time, the closed loop system is stable. If $V \geq c_2/c_1$, the situation turns to be the previous case. Therefore, we can conclude that the closed-loop system is asymptotically stable.

5. SIMULATION RESULTS

In this section, nonlinear numerical simulation results are presented to demonstrate the effectiveness of the proposed IGC controller. The superior performance of the proposed IGC controller is verified by comparing the performance to a finite time convergence(FTC) guidance law (Zhou et al. (2009)) plus three-loop autopilot structure and an IGC controller without adaptive terms(IGCWAT). Finally, Monte Carlo simulations are carried out to test the robustness of the proposed IGC controller.

5.1 Simulation Parameters and Physical Limited

The required kinematics are set as $R(0) = 1077$m, missile initial position $(0\text{m}, 16000\text{m})$, $\lambda(0) = 21.8\,\text{deg}$, $\gamma_M(0) = 0\,\text{deg}$, $\gamma_T(0) = 10\,\text{deg}$, $V_M = 3.5$Ma, where the Sonic is 297.05m/s, $V_T = 900$m/s, $a_T = 25\sin(0.6t)$ m/s. The missile dynamics in (3) and (8) are set as $\alpha(0) = 10\,\text{deg}$, $\omega_z(0) = 0$deg/s, $\theta(0) = 10\,\text{deg}$, $\tau_s = 0.01$, and the fin deflection angle is limited as $|\delta_z| \leq 30\,\text{deg}$. The nominal aerodynamic parameters are listed as follows (Hou et al. (2013); He et al. (2017b)):

$$C_{y,n}^{\alpha} = 0.3487, C_{y,n}^{\delta_z} = 0.068, M_{z,n}^{\alpha} = -17.801,$$
$$M_{z,n}^{\omega_z} = -0.2741, M_{z,n}^{\delta_z} = -31.267$$

The IGC controller parameters are set as follows:

$$k_1 = 0.8, k_2 = 10, k_3 = 10, k_4 = 50$$
$$r_1 = 0.3, r_2 = 1.5, r_3 = 1.5, r_4 = 2$$
$$\rho_1 = \rho_2 = \rho_3 = \rho_4 = 0.01$$

In order to alleviate the control command chattering, the discontinuous function $\text{sgn}(s)$ can be replaced by the sigmoid function (kumar and Ghose (2015))

$$sgmf(s) = 2\left(\frac{1}{1+\exp^{-as}} - \frac{1}{2}\right), a > 0 \qquad (35)$$

where the parameter a is chosen as 20.

5.2 Comparison with FTC Guidance Law Plus Three-loop Autopilot and IGC Controller without Adaptive Terms

The compared FTC guidance law is defined as

$$a_{mc} = -N\dot{R}\dot{\lambda} + a_{T\max}\text{sgn}\left(\dot{\lambda}\right) + \beta\left|\dot{\lambda}\right|^n \text{sgn}\left(\dot{\lambda}\right) \qquad (36)$$

where a_{mc} denotes the missile acceleration command, the other design parameters are set as: $N = 3.3$, $a_{T\max} = 25$, $\beta = 4$, $n = 0.5$. The three-loop autopilot is designed through the pole placement method. The compared IGCWAT is almost the same with IGC controller besides the adaptive terms $\hat{M}_1, \hat{M}_2, \hat{M}_3, \hat{M}_4$ turn into constants (Shima et al. (2006)), which we set as:

$$\hat{M}_1 = \hat{M}_2 = \hat{M}_3 = \hat{M}_4 = 0.1$$

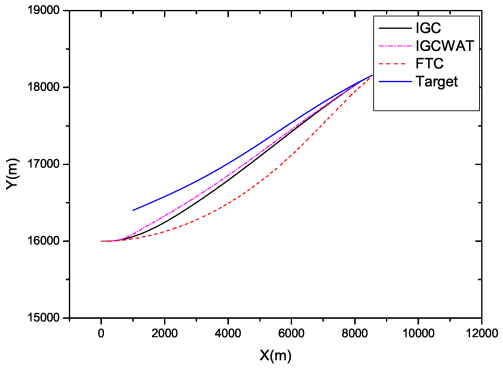

Fig. 2. Interception trajectories profiles of three guidance laws

The simulation results, including the interception trajectories, missile-target relative range profiles, LOS angular rates profiles, fin deflection angle commands, and missile accelerations of three different scenarios are present in Fig.2-6. The simulation trajectories presented in Fig.2 show that the proposed IGC controller can provide small miss distance interception in the presence of system uncertainties and target maneuvering. The recorded miss distances of the proposed IGC controller, IGCWAT and FTC guidance law plus three-loop autopilot in Fig.3 are 0.084m, 2.34m and 0.305m, respectively, demonstrate the superior performance of the proposed IGC controller. Fig.4 presents the LOS angular rate variation during the interception engagements obtained from three methods. It is obvious that the LOS angular rate of the proposed IGC controller converges to zero faster than the FTC guidance law. The LOS angular rate of IGCWAT controller converges to zero the same with proposed IGC controller at the beginning of the engagement. Due to the decrease of missile-target relative range and unknown target maneuver, the LOS angular rate of all methods diverge at the end of the interception engagement. The fin deflection angle commands are present in Fig.5. From this figure, it can be seen that the proposed IGC controller generates smoother command than other two methods. The missile acceleration response curves are shown in Fig.6, demonstrate that the proposed IGC controller can generate near-zero acceleration at the end of the interception, while the other two methods require large missile acceleration at the end of the interception engagement. Based on the results, we can conclude that the proposed IGC controller performs better than other two approaches.

5.3 Monte Carlo Simulation

Monte Carlo simulation method is introduced in this subsection to analyze the robustness of the proposed IGC controller against aerodynamic uncertainties, fin servo dynamic uncertainty and target maneuvering uncertainty. The parameters of the controller and the differentiator are the same with the previous case. The aerodynamic parameters $C_y^{\alpha}, C_y^{\delta_z}, M_z^{\alpha}, M_z^{\omega_z}, M_z^{\delta_z}$, fin servo time constant τ_s and target acceleration a_T have random variations within $\pm 10\%$ with respect to their nominal values.

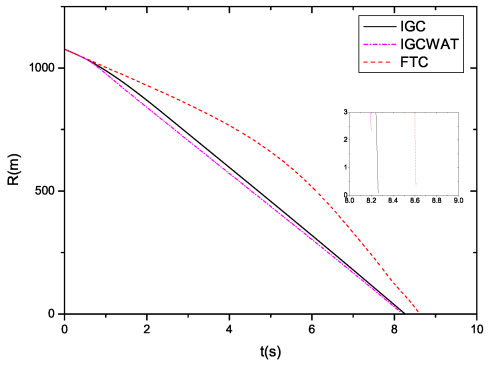

Fig. 3. Missile-target relative range profiles of three guidance laws

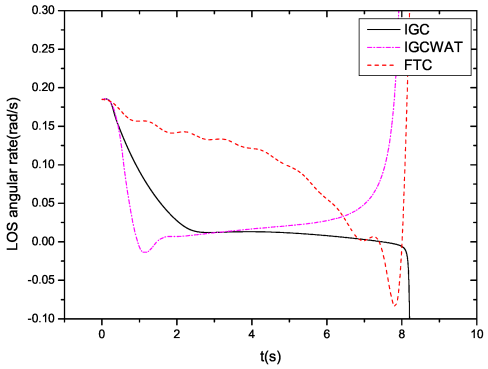

Fig. 4. LOS angular rates of three guidance laws

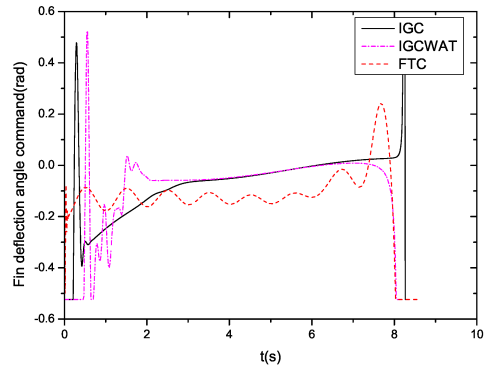

Fig. 5. Fin deflection angle commands of three guidance laws

The interception trajectories of 100 Monte Carlo runs are shown in Fig.7. The simulation results demonstrate that the proposed IGC controller provides an acceptable interception accuracy even with aerodynamic uncertainties, fin servo dynamic uncertainty and target maneuvering uncertainty. Through statistic calculations, the average miss distance is 0.1863m and the standard deviation of the miss distance is 0.1125m. The missile accelerations are presented in Fig.8. These results sufficiently demonstrate

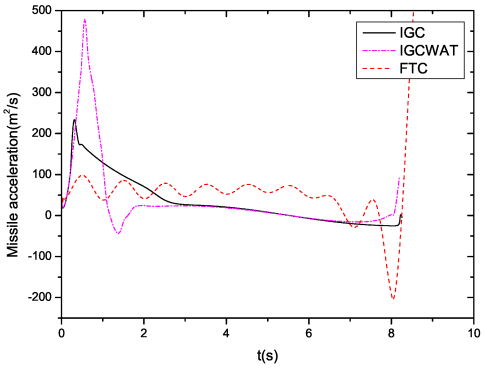

Fig. 6. Missile accelerations profiles of three guidance law

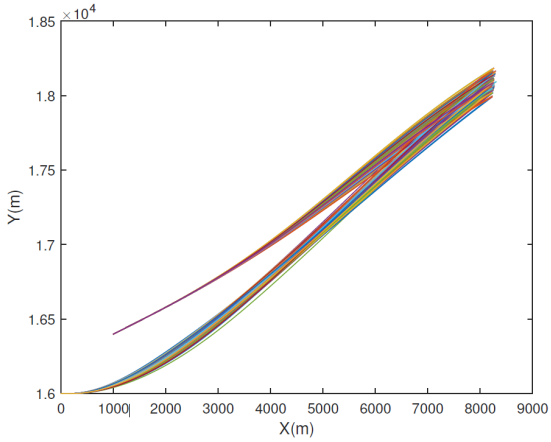

Fig. 7. Interception trajectories profiles of Monte Carlo simulations

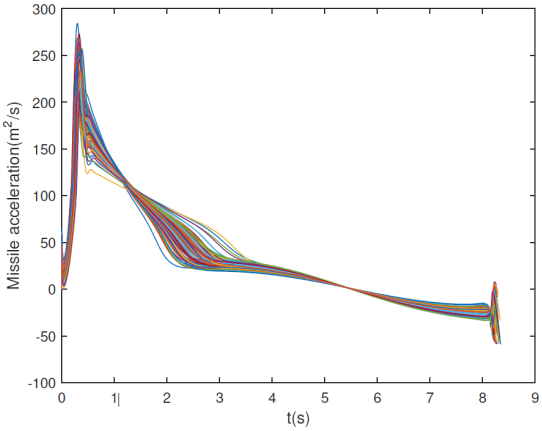

Fig. 8. Missile accelerations profiles of Monte Carlo simulations

that the proposed IGC controller is highly robust against several conventional uncertainties.

6. CONCLUSION

A novel integrated guidance and control controller is proposed for the terminal phase of intercepting a maneuvering target based on adaptive backstepping method and

SSOSMD in this paper. Fin servo dynamic and missile aerodynamic are taken into consideration by using the backstepping technique. By taking all uncertainties as disturbances and then compensating by adaptive terms, the proposed IGC controller requires no information on target maneuver in implementation. These properties provide the robustness against the model uncertainties. A novel SSOSMD is also proposed to calculate the derivatives of virtual control laws. This simplifies the formulations and avoids the explosion of terms in typical backstepping design. The closed-loop stability analysis is also proved by Lyapunov stability theory. Finally, simulation results with some comparison analysis and Monte Carlo simulations demonstrate the effectiveness and robustness of proposed integrated guidance and control law.

REFERENCES

Erdos, D., Shima, T., Kharisov, E., and Hovakimyan, N. (2012). *L1 Adaptive Control Integrated Missile Autopilot and Guidance*. Guidance, Navigation, and Control and Co-located Conferences. American Institute of Aeronautics and Astronautics.

Fei, L., Yang, K., and Ji, H. (2015). Adaptive integrated guidance and control with actuator failures based on backstepping and input-to-state stability. In *Guidance, Navigation and Control Conference*, 49–54.

He, S.M., Wang, W., and Lin, D.F. (2017a). Adaptive backstepping impact angle guidance law accounting for autopilot lag. *Journal of Aerospace Engineering*, 30(3).

He, S., Lin, D., and Wang, J. (2015a). Continuous second-order sliding mode based impact angle guidance law. *Aerospace Science and Technology*, 41, 199–208.

He, S., Lin, D., and Wang, J. (2015b). Robust terminal angle constraint guidance law with autopilot lag for intercepting maneuvering targets. *Nonlinear Dynamics*, 81(1), 881–892.

He, S., Song, T., and Lin, D. (2017b). Impact angle constrained integrated guidance and control for maneuvering target interception. *Journal of Guidance, Control, and Dynamics*, 40(10), 2653–2661.

Hou, M., Liang, X., and Duan, G. (2013). Adaptive block dynamic surface control for integrated missile guidance and autopilot. *Chinese Journal of Aeronautics*, 26(3), 741–750.

Idan, M., Shima, T., and Golan, O.M. (2007). Integrated sliding mode autopilot-guidance for dual-control missiles. *Journal of Guidance Control Dynamics*, 30(4), 1081–1089.

kumar, S.R. and Ghose, D. (2015). *Impact Time and Angle Control Guidance*. AIAA SciTech Forum. American Institute of Aeronautics and Astronautics.

Lin, C.F., Wang, Q., Spayer, J.L., Evers, J.H., and Cloutier, J.R. (1992). Integrated estimation, guidance, and control system design using game theoretic approach. 4, 3220–3224.

Menon, P.K., Sweriduk, G.D., Ohlmeyer, E.J., and Malyevac, D.S. (2004). Integrated guidance and control of moving-mass actuated kinetic warheads. *Journal of Guidance, Control, and Dynamics*, 27(1), 118–126.

Omar, H.M. and Abido, M.A. (2010). Designing integrated guidance law for aerodynamic missiles by hybrid multi-objective evolutionary algorithm and tabu search. *Aerospace Science and Technology*, 14(5), 356–363.

Panchal, B., Mate, N., and Talole, S.E. (2017). Continuous-time predictive control-based integrated guidance and control. *Journal of Guidance, Control, and Dynamics*, 40(7), 1579–1595.

Park, B.G., Kim, T.H., and Tahk, M.J. (2011). Time-delay control for integrated missile guidance and control. *International Journal of Aeronautical Space Sciences*, 12(3), 260–265.

Phadke, S.B. and Talole, S.E. (2012). Sliding mode and inertial delay control based missile guidance. *IEEE Transactions on Aerospace and Electronic Systems*, 48(4), 3331–3346.

Ran, M., Wang, Q., Hou, D., and Dong, C. (2014). Backstepping design of missile guidance and control based on adaptive fuzzy sliding mode control. *Chinese Journal of Aeronautics,*, 27(3), 634–642.

Shima, T., Idan, M., and Golan, O.M. (2006). Sliding-mode control for integrated missile autopilot guidance. *Journal of Guidance Control Dynamics*, 29(2), 250–260.

Shtessel, Y.B. and Tournes, C.H. (2009). Integrated higher-order sliding mode guidance and autopilot for dual control missiles. *Journal of Guidance Control Dynamics*, 32(1), 79–94.

Vaddi, S., Menon, P.K., and Ohlmeyer, E.J. (2009). Numerical state-dependent riccati equation approach for missile integrated guidance control. *Journal of Guidance, Control, and Dynamics*, 32(2), 699–703.

Wang, J., Liu, L., Wang, P., and Tang, G. (2016a). Guidance and control system design for hypersonic vehicles in dive phase. *Aerospace Science and Technology*, 53(Supplement C), 47–60.

Wang, W., Xiong, S., Wang, S., Song, S., and Lai, C. (2016b). Three dimensional impact angle constrained integrated guidance and control for missiles with input saturation and actuator failure. *Aerospace Science and Technology*, 53(Supplement C), 169–187.

Wei, Y., Hou, M., and Duan, G.R. (2010). Adaptive multiple sliding surface control for integrated missile guidance and autopilot with terminal angular constraint. In *Control Conference*, 2162–2166.

Xin, M., Balakrishnan, S.N., and Ohlmeyer, E.J. (2006). Integrated guidance and control of missiles with theta-d method. *IEEE Transactions on Control Systems Technology*, 14(6), 981–992.

Yan, H., Wang, X., Yu, B., and Ji, H. (2014). Adaptive integrated guidance and control based on backstepping and input-to-state stability. *Asian Journal of Control*, 16(2), 602–608.

Zarchan, P. (2012). Tactical and strategic missile guidance, sixth edition. *American Institute of Aeronautics Astronautics Inc*, (6), 555.

Zhang, B. and Song, S. (2009). Integrated playback design of missile guidance and control based on adaptive sliding-mode control. *Journal of Projectiles Rockets Missiles Guidance*, 29(5), 31–35.

Zhou, D., Sun, S., Teo, K.L., Zhou, D., and Sun, S. (2009). Guidance laws with finite time convergence. *Journal of Guidance Control Dynamics*, 32(6).

Zhou, D. and Xu, B. (2016). Adaptive dynamic surface guidance law with input saturation constraint and autopilot dynamics. *Journal of Guidance, Control, and Dynamics*, 39(5), 1155–1162.